Bulletin of the Seismological Society of America, Vol. 89, No. 1, pp. 250–259, February 1999

Microtremor Measurements Used to Map Thickness of Soft Sediments

by Malte Ibs-von Seht and Jürgen Wohlenberg

Abstract The observations about the behavior of microtremor spectra presented here show that noise measurements can be used as a powerful tool to determine the thickness of soft cover layers. The most suitable method for this determination is Nakamura's technique, which is the ratio of the horizontal-component noise spectrum and that of the vertical component (H/V spectrum). The frequency of the main peak in these spectral ratios correlates well with the sediment thickness at the site. Using an extensive database of microtremor measurements carried out in the western Lower Rhine Embayment (Germany), it was possible to show that this correlation is clearly valid for a wide range of thickness, namely, from tens of meters to more than 1000 m. A simple formula was derived that, for the sediments to be found in the area investigated, directly calculates the cover thickness from the frequency of the main peak in the H/V spectrum. A comparison with calculated resonant frequencies suggests the relation derived from the noise measurements depending on the velocity depth function of the shear wave. Classical spectral ratios are shown to be strongly influenced by the noise level and are therefore less reliable in determining the resonant frequency of the subsoil. The practical relevance of the investigation is illustrated by means of cross sections, constructed from results of the microtremor analyses, which provide a convincing image of the surficial structure of the areas investigated.

Introduction

The term microtremor summarizes all ground vibrations not due to events of short duration, such as earthquakes or explosions (Steinwachs 1974). In this article, we use the term *seismic noise* as a synonym. The sources of seismic noise and its typical frequencies are manifold: sea waves and coastal surf produce long-period ground movements, while wind and rainfall cause vibrations of higher frequencies. In urban regions, human noise caused by traffic and industrial activities predominates. Seismic noise measured on the Earth's surface is subject to temporal and regional variations. Sea waves cause a seasonal effect on the low-frequency part of the spectra (approx. 0.1 Hz) (Aki and Richards, 1980). Human noise shows a daily rhythm and mainly influences frequencies above 1 Hz. Regional changes in noise result from the variation in distance to different sources but also from the influence the site subsurface has on the noise spectra. Following earthquake seismology terminology, a noise spectrum measured at a site generally can be taken as a superposition of source influences (source effect) and subsoil influences (site effect).

Site effects may cause amplification of seismic waves during earthquakes, thus being of special interest in engineering seismology. Since the 1950s, attempts have been made to obtain information about soil amplifications using recordings of ambient seismic noise, resulting mainly in two techniques based on the spectral analysis of the noise recordings. Both methods provide a spectrum in some way related to the transfer function of a site by forming the ratio of certain noise spectra (Field and Jacob, 1993; Lermo and Chávez-García, 1994).

It should be mentioned that it is not our aim to investigate spectral ratio methods theoretically. Our study investigates the application of two spectral ratio techniques, originally designed for site response evaluations, for obtaining geological information about the subsoil. The study was motivated by the fact that the transfer function of a sediment site is closely connected to the structure and the geotechnical parameters of the subsurface layers, namely, its thicknesses and shear-wave velocities. Therefore, it should be possible to determine sediment thicknesses using these techniques.

Basics

The site effect is given in terms of a transfer function. A simple two-layer model explains its basic principle (Fig. 1): A hardrock basement is covered by a soft sedimentary layer of thickness m and shear-wave velocity v_s. Resonant frequencies of this system occur for thicknesses that are uneven multiples of $\lambda/4$. The transfer function has maxima at frequencies

$$f_r = \frac{n \cdot v_s}{4m} \quad (n = 1, 3, 5, \ldots). \tag{1}$$

A velocity-depth function in a sedimentary layer may be written as

$$v_s(z) = v_0 \cdot (1 + Z)^x, \tag{2}$$

where v_0 is the surface shear-wave velocity, $Z = z/z_0$ (with $z_0 = 1m$), and x gives the depth dependence of the velocity. The fundamental resonant frequency f_r is calculated as $1/4T_0$, where T_0 is the shear-wave travel time between the bottom of the layer and the surface. As by definition, $v(z) = dz/dt$, the travel time is calculated as

$$T_0 = \int_0^m \frac{dz}{v_s(z)} = \frac{1}{v_0} \int_0^m (1 + Z)^{-x}\, dz = \frac{1}{v_0} \frac{(1 + m)^{1-x} - 1}{(1 - x)}. \tag{3}$$

The dependency between thickness and resonant frequency becomes

$$f_r = \frac{1}{4T_0} = \frac{v_0(1 - x)}{4[(1 + m)^{1-x} - 1]} \tag{4}$$

or

$$m = \left[\frac{v_0(1 - x)}{4f_r} + 1\right]^{1/(1-x)} - 1, \tag{5}$$

where f_r is to be given in Hz, v_0 in m/sec, and m in m.

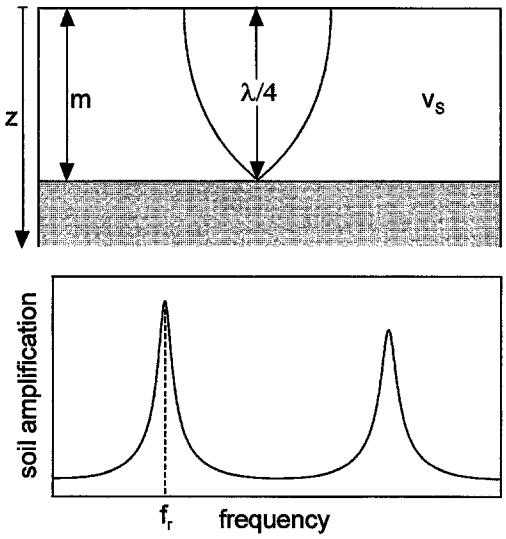

Figure 1. Basic principle of site response, transfer function.

Shear-wave velocities of the sediments to be found in the area of investigation were experimentally determined by Budny (1984) using downhole measurements. For the sandy lithology in the western Lower Rhine Embayment, he gives values for the surface velocity $v_0 = 162$ m/sec and the depth dependence $x = 0.278$. Figure 2 is a plot showing equation (5) with these values. We presuppose that the shear-wave velocity of the half-space is always higher than in the cover layer because otherwise there would be no resonance at all.

Under ideal conditions, the thickness of a layer could be calculated from its measured resonant frequency on the basis of the shear-wave velocity. Problems occur because in most cases resonant frequencies cannot be read directly from noise spectra. Rather, the spectra are superimposed by the influences of the source effect, namely, the frequency content and the amplitudes of the microtremor sources. There are two techniques that use spectral ratios of microtremors to overcome this problem (Fig. 3). The first method, sometimes called classical spectral ratio technique, uses a remote

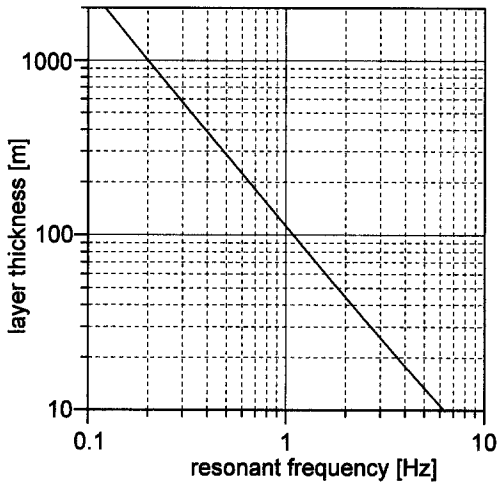

Figure 2. Connection between layer thickness and resonant frequency calculated on the basis of equation (5).

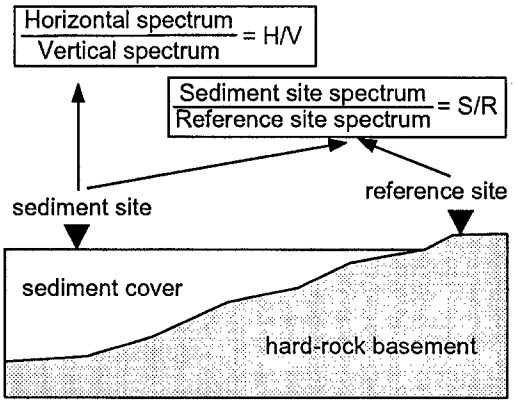

Figure 3. Two techniques for site response evaluations using noise spectra.

reference recording site placed on hard rock and a second recorder that is placed on the sediments to be mapped. The spectral ratio of noise recordings at the two sites is assumed to show something similar to the site effect (Lermo *et al.*, 1988; Field and Jacob, 1990; Field *et al.*, 1995; Lachet *et al.*, 1996). We call this kind of spectral ratio S/R spectrum (because the spectral ratio of a sediment site and a reference site is formed). The second method, proposed by Nakamura (1989) and known as Nakamura's technique, requires only one recording station. This is because the spectral ratio of the horizontal and the vertical components recorded at the same site is formed (H/V spectrum). This process is said to eliminate the influence of the source effect. A more detailed description of the method can be found in Lermo and Chávez-García (1993).

Nakamura's technique has awakened interest because it seems to show some essential advantages over traditional S/R spectra. Nakamura (1989), Lermo and Chavez-Garcia (1993), Field *et al.* (1995), and Lachet *et al.* (1996) applied the method for site response estimations in Japan, Europe, and America. They found out that determination of the fundamental resonant frequency of the subsoil is possible. In contrast to classical S/R spectra, Nakamura's technique should also allow a rough estimate of the soil amplification factor. In field practice, Nakamura's technique is less expensive, because only one recording station is needed, and it is said to be less sensitive to local noise sources. A satisfactory theoretical explanation of the method has not yet been given. Lachet and Bard (1994) investigated the method using numerical noise simulations. They conclude that H/V spectra show clear maxima at the resonant frequency of the subsoil, but its amplitudes are dependent on the Poisson's ratio of the uppermost layer and are therefore not suitable for soil amplification estimates. Further theoretical support has been given by Field and Jacob (1995).

Field Data

Microtremor measurements were carried out in two boundaried areas of the western Lower Rhine Embayment (Germany) to the north of Aachen (Fig. 4). The geological evolution of this region has produced sedimentary covers of different thicknesses of Tertiary and Quaternary ages. The southern area of investigation (Fig. 5, *top*) covers the northern border of the Eifel, where the Paleozoic basement dips toward the north. The soft-rock thicknesses increase from 0 m in the south to about 350 m in the north. The northern area of investigation (Fig. 5, *bottom*) is situated in a region where sediment thickness is much higher and may exceed 1000 m. The various layer thicknesses are crucial for the study because they produce the various spectral responses observed. One further advantage of the areas investigated is the large number of drilling sites. At these points, detailed information about the subsurface structure, namely, the thickness of sedimentary covers, is available. This is needed for calibrating the results of the noise investigations.

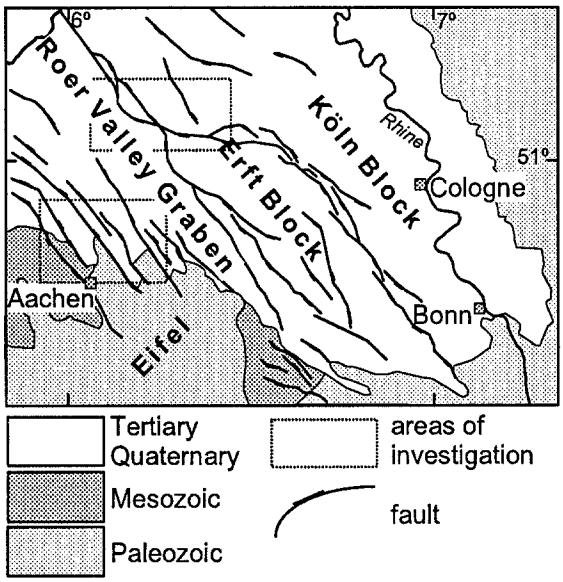

Figure 4. Geological overview of the western Lower Rhine Embayment and areas of investigation.

We present here the results of measurements at 102 sites. Thirty-four of them were made very close to or directly at drilling sites where the cover thickness is known. Ten sites were placed on hard rock and used as reference stations for the forming of S/R spectra. To minimize the influence of human noise, all recordings were taken at night between 1 a.m. and 4 a.m. We used digital equipment (Lennartz PCM 5800) and three different seismometer types (Mark L4-3D/1 second, Lennartz LE-3D/1 second, and LE-3D/5 second). Table 1 gives the labels and the coordinates of the sites.

For further processing, only quiet sections of the noise recordings were used. Therefore, all recordings were examined to identify and cut off those parts of the traces disturbed by very near-local sources, such as passing cars or operator's footsteps. The resulting length of the clean recordings varies between 1 and 10 min and is given in Table 1. During data processing, an instrument correction was applied to those recordings taken by 1-sec seismometers to obtain a flat response above approx. 0.5 Hz. Amplitude spectra were calculated for all sites and components. The spectra were smoothed by applying a low-pass filter. Furthermore, rms amplitudes of the noise recordings were calculated for all traces (see Table 1).

The H/V spectral ratio $[T_{H/V}(\omega)]$ was obtained by dividing the averaged spectra of the horizontal components of the sediment site $[S_{NS}(\omega)$ and $S_{EW}(\omega)]$ by the spectrum of the vertical component $[S_V(\omega)]$ of the sediment site:

$$T_{H/V}(\omega) = \frac{[S_{NS}(\omega) + S_{EW}(\omega)]/2}{S_V(\omega)}. \quad (6)$$

The S/R spectral ratio $[T_{S/R}(\omega)]$ was formed by dividing the averaged spectra of the horizontal components of the sedi-

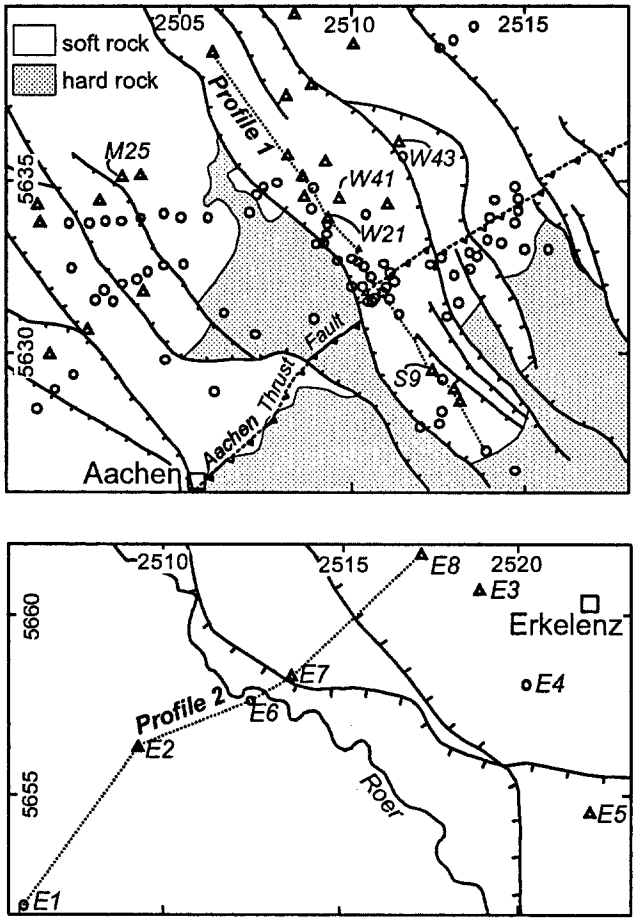

Figure 5. Areas of investigation: locations of sites measured (circles and triangles, triangles are sites with information from drillings). (*top*) Southern area of investigation. (*bottom*) Northern area of investigation. For clarity, solely sites mentioned in the text are labeled.

ment site by an averaged spectrum of the averaged horizontal component spectra [$R_{NS}(\omega)$ and $R_{EW}(\omega)$] of the 10 hard-rock (reference) sites [$\bar{R}_H(\omega)$]:

$$T_{S/R}(\omega) = \frac{[S_{NS}(\omega) + S_{EW}(\omega)]/2}{\bar{R}_H(\omega)} \quad (7)$$

with

$$\bar{R}_H(\omega) = \left[\sum_{i=1}^{10} R_{NS}(\omega)(i) + \sum_{i=1}^{10} R_{EW}(\omega)(i)\right]/20. \quad (8)$$

Results

First, transfer functions were calculated for some sites where the structure of the layered subsurface was known from drillings. The transfer functions should be compared with the noise S/R and H/V spectra. Theoretical transfer

Table 1
Coordinates of Sites Measured and Results of Microtremor Analysis

Site	G	t (sec)	R (km)	H (km)	rms_H (nm/sec)	$f_{(S/R)}$ (Hz)	$f_{(H/V)}$ (Hz)	m_{drill} (m)	m_{calc} (m)
W1	S	116	2507.83	5634.92	350	1.65	0.72		151
W2	S	137	2508.90	5634.82	283	1.61	0.64	155	178
W3	S	46	2508.83	5634.18	336	1.60	0.80		131
W4	S	143	2510.42	5634.02	251	1.40	0.92	100	108
W5	H	71	2508.98	5633.15	213	2.90			
W6	S	134	2510.68	5631.58	112	2.90	2.28		31
W7	S	133	2510.45	5631.47	163	3.20	3.32		18
W8	H	171	2508.90	5631.00	73				
W9	H	89	2507.19	5630.53	142				
W10	S	115	2506.30	5631.15	90		4.64	15	11
W12	S	174	2510.21	5633.03	202	1.30	1.04	97	91
W13	S	110	2510.00	5632.72	196	1.30	1.20		75
W14	H	179	2509.58	5632.67	151				
W15	H	222	2507.03	5634.08	146				
W16	H	60	2507.22	5634.60	97				
W17	S	150	2507.45	5634.82	360	1.35	0.76		140
W18	S	216	2509.18	5633.18	172	1.30	1.05		90
W19	S	180	2509.25	5633.44	252	1.10	0.84		122
W20	S	126	2509.31	5633.73	285	1.15	0.84		122
W21	S	204	2509.33	5633.94	291	1.15	0.80	112	131
W22	S	132	2510.59	5631.48	141	3.70	2.80		23
W23	S	114	2510.91	5631.75	171	3.75	2.80		23
W24	S	192	2511.00	5631.90	191	3.70	2.64		25
W25	S	216	2511.24	5632.07	171	3.05	2.96		21
W26	S	144	2511.10	5632.32	179	2.85	2.12		34
W27	S	78	2510.67	5632.00	203	3.30	2.92		22
W28	S	186	2510.32	5631.90	122	4.30	2.44		28
W29	H	204	2509.99	5631.90	86				
W30	S	186	2510.92	5632.57	169	1.60	1.64		48
W31	S	186	2510.55	5632.20	144	1.65	2.40		29
W32	S	186	2510.35	5632.51	158	1.40	1.48		56
W33	S	186	2510.19	5632.63	151	1.30	1.28		68
W34	S	144	2511.87	5630.44	1002	3.10	2.52		27
W35	S	55	2511.38	5631.11	228	5.00	2.70		24
W36	S	174	2511.09	5631.55	189	2.70	3.32		18
W37	S	394	2508.64	5634.54	555	1.80	0.64	168	178
W38	S	569	2508.58	5635.16	355	1.20	0.64	161	178
W39	S	354	2508.15	5635.76	512	1.35	0.60	158	195
W40	S	365	2509.24	5635.58	295	1.15	0.76	140	140
W41	S	882	2509.64	5634.50	258	1.10	0.84	140	122
W42	S	553	2511.04	5634.34	286	1.20	1.08	92	86
W43	S	451	2511.38	5636.13	256	1.55	1.36	61	63
S1	H	88	2511.98	5627.87	490				
S2	S	40	2512.54	5627.95	688	1.40	0.92		108
S3	S	96	2512.61	5628.32	353	1.35	0.76		140
S4	S	141	2513.15	5628.60	260	1.50	1.36	58	63
S5	S	106	2513.88	5627.20	296	2.20	2.20		32
S6	H	210	2514.68	5626.64	93				
S7	S	186	2512.96	5628.99	678	1.90	1.40	56	60
S8	S	72	2512.63	5629.25	1046	3.00	1.80		42
S9	S	44	2512.32	5629.50	782	4.10	1.60	55	50
A1	S	253	2513.55	5639.43	947	0.55	0.36	365	396
A2	S	173	2512.95	5639.04	809	1.40	0.40	365	342
A3	S	345	2512.56	5638.81	792		0.56		215
A4	S	117	2511.50	5635.71	238	1.60	1.44		58
A5	S	599	2510.08	5638.92	292	1.25	0.89	111	113
A6	S	489	2508.37	5639.76	347	1.00	0.80	154	131
A7	S	499	2508.83	5637.77	379	1.20	0.52	205	238
A8	S	316	2508.10	5637.46	309	0.70	0.70	190	157
A9	S	561	2506.02	5638.67	881		0.68	161	164

(*continued*)

Table 1
Coordinates of Sites Measured and Results of Microtremor Analysis (*continued*)

Site	G	t (sec)	R (km)	H (km)	rms_H (nm/sec)	$f_{(S/R)}$ (Hz)	$f_{(H/V)}$ (Hz)	m_{drill} (m)	m_{calc} (m)
M7	S	101	2502.84	5633.84	176	1.45	1.35		55
M8	S	180	2503.90	5633.90	62		3.20		19
M10	S	192	2502.36	5633.78	247	1.30	1.12		82
M11	S	195	2503.33	5633.81	215	1.60	1.20		75
M12	S	198	2504.55	5634.04	108	2.60	2.68		24
M13	S	168	2505.03	5633.93	79	3.10	2.80		23
M14	S	189	2505.83	5633.95	85		7.96		5
M16	S	180	2503.34	5631.98	232	3.00	1.10		84
M17	S	246	2503.75	5632.12	590	2.80	1.32		65
M18	S	288	2504.08	5632.33	167	1.70	1.52		54
M19	S	300	2504.53	5632.51	127	2.30	2.32		30
M20	S	258	2505.10	5632.56	114	2.00	1.96		38
M23	S	318	2504.00	5631.78	214	1.30	1.12	87	82
M24	S	429	2502.70	5634.42	258	1.60	1.36	67	63
M25	S	224	2503.36	5635.13	322	2.10	2.20	44	32
M26	S	323	2503.90	5635.17	107		4.50	30	12
J2	H	309	2515.70	5633.00	64				
J3	S	552	2515.00	5633.01	118		3.60		12
J4	S	664	2514.33	5633.18	102		4.10		11
J5	S	309	2513.42	5632.91	186	1.70	1.62		
J6	S	309	2512.60	5632.76	99				
J7	S	428	2512.28	5632.55	220		2.05		31
J8	S	540	2513.93	5633.28	207		2.12		34
J9	S	540	2513.63	5632.79	125		5.00		10
J10	S	397	2513.43	5632.43	108	1.35	1.05		90
J11	S	292	2512.96	5632.25	105		1.10		84
J12	S	540	2513.08	5631.45	256	4.10	4.00		14
J13	S	327	2512.75	5631.05	451	1.34	0.95		103
J14	S	336	2514.72	5633.78	67	5.45	5.55		9
J15	S	329	2514.82	5634.15	228	4.40	4.48		12
J16	S	531	2514.81	5634.50	196	4.40	4.48		12
J17	S	419	2514.72	5634.84	271	3.66	3.60		16
J18	S	129	2514.14	5634.45	86	4.12	3.92		14
J19	S	312	2513.99	5633.93	64				
E1	S	282	2506.12	5651.93	548		0.20	900	895
E2	S	518	2509.45	5656.50	649		0.16	1257	1219
E3	S	381	2518.88	5660.77	701		0.28	549	561
E4	S	250	2520.18	5658.08	681		0.40	500	342
E5	S	391	2522.00	5654.60	636		0.28	565	561
E6	S	543	2512.50	5657.72	760		0.14	1600	
E7	S	453	2513.65	5658.33	857		0.79	177	
E8	S	546	2517.23	5662.28	700		0.37	460	

Site = label of site; G = geology; S = soft rock; H = hard rock; R and H = longitude and latitude according to Gauss–Krueger coordinates; rms_H = averaged horizontal rms amplitude; $f_{(S/R)}$ = frequency of main peak in S/R spectrum; $f_{(H/V)}$ = frequency of main peak in H/V spectrum; m_{drill} = thickness of cover layer known from drilling (if available); m_{calc} = thickness of cover layer calculated using H/V frequencies.

functions were computed using the method proposed by Haskell (1960). The geotechnical parameters required were taken from Budny (1984). He experimentally determined $v_s(z)$ functions and Q factors for different soft rocks of the Lower Rhine Embayment. Furthermore, he gives density values for these rocks.

Figure 6 shows examples of calculated transfer functions compared with S/R and H/V spectra for six different sites (for model parameters, see Table 2). The plots show clear similarities between the different types of spectra. The spectral ratios always have dominant maxima at low frequencies that correspond to the main peak in the transfer functions. Furthermore, the general decay of the transfer functions toward high frequencies is also visible in the spectral ratios. Sites S9 and E5 are exceptions. In the case of these stations, neither the frequency nor the amplitude of the main peak of the S/R spectral ratios show similarities with the transfer functions. Site S9 was situated in the vicinity of a high-density traffic highway, the high-noise amplitudes of which obviously spoil the shape of the S/R spectrum. E5 is a site of high sedimentary thickness (565 m), which appears to be the reason why the information content of the S/R spectrum is low. In contrast, these factors seem to have little or no effect on the H/V spectra.

When calculating transfer functions, problems occur because the thickness and lithology of the sedimentary layers may be known, but geotechnical parameters have to be taken from empirical formulas. In fact, at an actual site, these parameters may vary considerably. Adjusting the parameters to obtain a shape similar to the spectral ratios is possible, but no new information is obtained in this way. We chose a different approach and looked at the correlation between the thickness at a site and the main frequency in the spectral ratios. For this purpose, the frequency of the main peak in the two types of spectral ratios was determined for all sedimentary sites (see Table 1). The data obtained at 34 drilling sites where the thickness was known are suitable for performing the correlation.

In Figure 7, the data of the drilling sites were used to plot the S/R and H/V main frequencies versus the thickness at the sites. S/R spectra sometimes do not show a clear main peak, resulting in a smaller number of data points for this kind of spectral ratio. The cross-plot reveals good correlation for the H/V frequencies over a wide range of thickness, namely, from tens of meters to more than 1000 m, while the S/R frequencies are more scattered. Furthermore, there are several S/R data points that have to be treated as outliers. These data points (indicated in the plot) were zero-weighted when calculating nonlinear regression fits of the form

$$m = af^b. \tag{9}$$

Values and standard errors of the correlation coefficients a and b are given in Table 3.

The relationships between the mean thickness m and the frequency of the main peak in S/R spectra, $f_{(S/R)}$, and H/V spectra, $f_{(H/V)}$, are given in equations (10) and (11).

$$m = 146 f_{(S/R)}^{-1.375}, \tag{10}$$

$$m = 96 f_{(H/V)}^{-1.388}, \tag{11}$$

The resulting straight lines are nearly parallel, and the S/R line is slightly shifted toward higher frequencies.

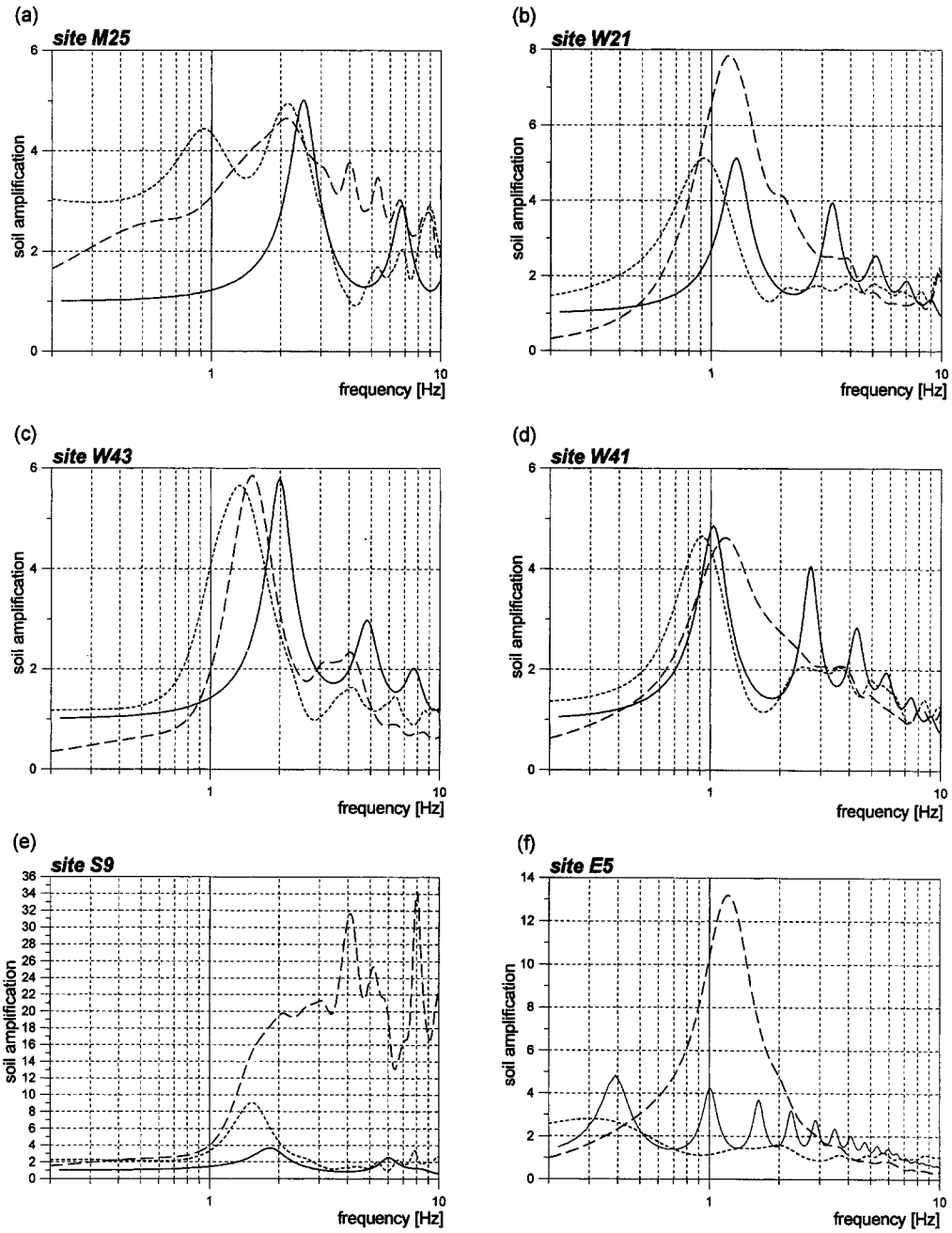

Figure 6. Spectral ratios of noise recordings compared with transfer functions calculated using parameters given in Table 2. Solid line: transfer function calculated; dashed line: S/R spectrum; dotted line: H/V spectrum.

Discussion

The good correlation between the main peak in the spectral ratios and cover thickness (at least concerning H/V frequencies) leads to the hypothesis that maxima in the spectral ratios are controlled by mechanisms that are similar or equal to those applied when calculating transfer functions. Comparison between (10) and (11), respectively, with the dependence between layer thickness and resonant frequency (5) gives further confirmation of this hypothesis. The graph of this dependence, also plotted in Figure 7, is approx. parallel to (10) and (11) and fits very well the H/V data points.

The frequency shift between S/R and H/V frequencies was also observed by Field and Jacob (1993). They found values of approx. 10% lowered H/V frequencies. Figure 8 is a cross-plot of S/R and H/V frequencies. A linear regression fit through the origin and the data points has a slope of 0.87 $\pm$ 0.06. This gives a value of approx. 13% shift between S/R and H/V frequencies and fits the observations of Field and Jacob (1993).

Table 2
Geotechnical Parameters Used to Calculate Transfer Functions for Sites M25, W21, W43, W41, S9, and E6

Site	Lithology	Depth (m)	v_s (m/sec)	ρ (kg/m^3)	Q
M25	clay	0–10	303	2053	6.1
	sand	10–25	398	2090	8.5
	sand	25–44	465	2101	10.4
	hard rock	>44	2500	2500	100
W21	loess	0–8	200	1900	3.5
	gravel	8–14	300	2080	6
	sand	14–25	398	2090	8.5
	sand	25–50	482	2104	10.9
	sand	50–75	540	2112	12.6
	sand	75–100	585	2117	14
	sand	100–111	622	2120	15.2
	hard rock	>111	2500	2500	100
W43	loess	0–8	200	1900	3.5
	gravel	8–15	300	2080	6
	sand	15–25	398	2090	8.5
	sand	25–50	482	2104	10.9
	sand	50–61	540	2107	12.6
	hard rock	>110	2500	2500	100
W41	loess	0–8	200	1900	3.5
	gravel	8–14	300	2080	6
	sand	14–25	398	2090	8.5
	sand	25–50	482	2104	10.9
	sand	50–75	540	2112	12.6
	sand	75–100	585	2117	14
	sand	100–129	622	2120	15.2
	clay	129–140	475	2298	16.2
	hard rock	>140	2500	2500	100
S9	sand	0–25	398	2090	8.5
	sand	25–33	430	2095	9.4
	brown coal	33–35	216	1200	3
	sand	35–55	495	2104	11.3
	hard rock	>55	2500	2500	100
E6	gravel	0–15	353	1800	6
	gravel	15–25	410	1950	8
	gravel	25–35	452	2050	10
	sand	35–50	482	2102	10.9
	sand	50–100	585	2113	14
	sand	100–150	654	2118	16.2
	sand	150–200	709	2122	18
	sand	200–250	754	2124	19.5
	sand	250–300	793	2125	20.9
	sand	300–350	828	2127	22
	sand	350–400	859	2127	23.1
	sand	400–450	888	2128	24.1
	sand	450–485	907	2129	24.8
	sand	485–520	600	3000	25.4
	sand	520–565	946	2129	26.2
	hard rock	>565	3100	2800	120

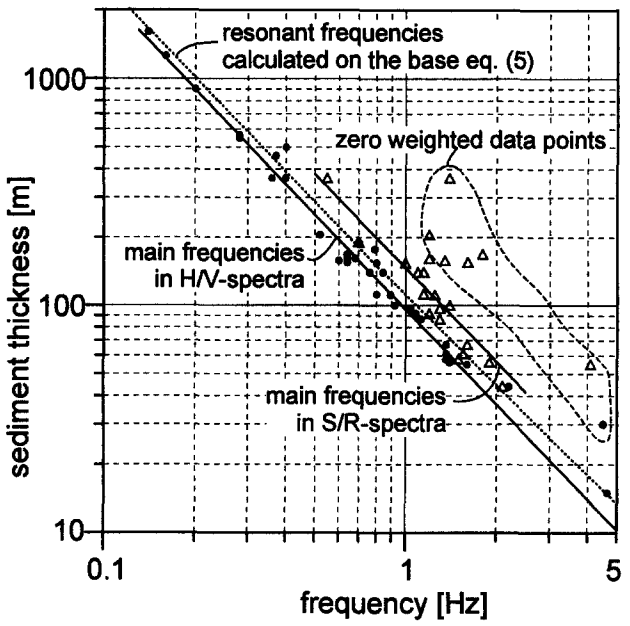

Figure 7. Main frequencies in spectral ratios plotted versus sediment thickness (solid circles: H/V frequencies; triangles: S/R frequencies). The solid lines are fits to the data points (see equation 9). The dashed line is the theoretical dependence between thickness and resonant frequency (see equation 5).

Table 3
Squared Correlation Coefficient (R_S) of Data Points in Figure 7 and Values of a and b in Equation (9) with Standard Errors (Δa and Δb)

	S/R Spectra	H/V Spectra
R_S	0.749	0.981
a	146	96
Δa	19	4
b	−1.375	−1.388
Δb	0.210	0.025

The deviations of the data points in Figure 7 from the strict linear relationships are most probably a consequence of lithological inhomogeneties. Equations (10) and (11) are based on the assumption of equal $v_s(z)$ functions at each site measured. Conditions in practice are different because there may occur layers of velocities more or less deviating from a general velocity-depth function. Thus, drawing a straight line through the data points includes an averaging of lithology or an averaging of the depth dependence of the shear-wave velocity. A thickness value calculated from (10) or (11) for a particular site can only be as reliable as the overall $v_s(z)$ function is valid for the site. The very local subsurface velocity structure cannot be taken into account for the calculation. However, especially for the H/V frequencies, the thickness-frequency correlation delivers an estimate of the local thickness that can be used for hard-rock basement mappings.

A reason for the numerous outliers of S/R frequencies in Figure 7 and the high scatter of the data points in Figure 8 could be the value of the noise level at the recording sites. Therefore, in Figure 9, we plotted the frequency ratio $f_{(S/R)}/f_{(H/V)}$ versus the horizontal rms amplitudes of the noise recordings (the amplitudes of the two horizontal records were averaged). The cross-plot illustrates that the frequency ratio becomes unstable and generally tends to higher values at

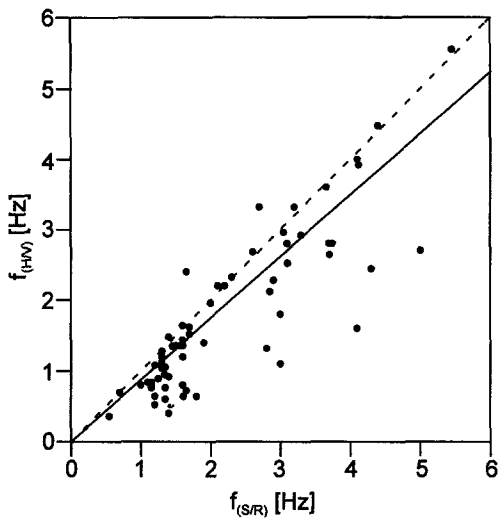

Figure 8. Plot of H/V main frequency [$f_{(H/V)}$] versus S/R main frequency [$f_{(S/R)}$]. The dashed line is the $f_{(H/V)} = f_{(S/R)}$ line.

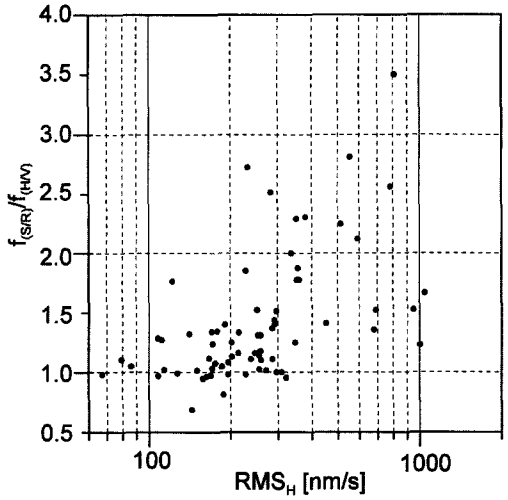

Figure 9. Ratio of S/R and H/V main frequencies plotted versus the rms horizontal amplitude of noise recordings.

increasing noise amplitudes. As a consequence, one of the two methods (S/R or H/V) seems to be affected by the noise level, which, in urban regions, mainly depend on the intensity of local noise sources. To find out which of the two methods is influenced by the noise level, we looked at the relation between the thickness calculated using (10) and (11) and the sediment thickness known from drillings with respect to the noise amplitudes. For this purpose, ratios of actual (m_{drill}) and calculated sediment thicknesses (m_{calc}) were formed. These ratios were plotted versus the rms amplitudes (Fig. 10). The thickness ratios derived from the H/V frequencies vary between 0.8 and 1.4, revealing no dependence on the noise amplitude. In contrast, the ratios de-

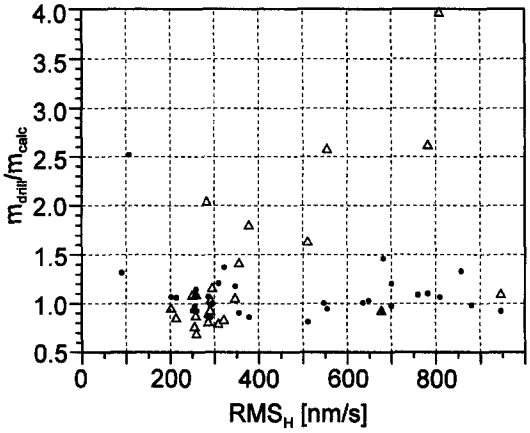

Figure 10. Ratio of actual (m_{drill}) and calculated (m_{calc}) thickness plotted versus the rms horizontal amplitude of noise recordings (solid circles: m_{calc} calculated using H/V frequencies; triangles: m_{calc} calculated using S/R frequencies).

rived from the S/R frequencies reach values up to 4 with increasing amplitude. This indicates that the frequencies of the main peaks in the S/R spectra are being influenced by local noise sources, while they are not controlled by the thickness of the cover layer.

The observed sensitivity of the S/R spectra to local noise sources can be explained as follows. As the thicknesses calculated on the base of (10) are too small, the frequencies $f_{(S/R)}$ measured are too high. This corresponds to the fact that smaller distances to noise sources cause increasing noise amplitudes, while the portion of high frequencies in the signal spectrum grows. As a consequence, high-frequency peaks occur in the numerator spectrum. The denominator spectrum provided by the reference site is not normally influenced by the same local noise source. Therefore, the high-frequency part of the spectrum is not eliminated during the formation of the S/R spectral ratio giving rise to the high-frequency main peaks in the S/R spectra. One could consider the conditions being reversed, that is, the reference site being influenced by near-noise sources while the sediment site is quiet. This would result in a spectral ratio that provides distinct local minima at high frequencies. In practice, such conditions are not normally given, because reference sites are situated preferably at quiet locations without local noise sources.

In the case of the H/V spectra, both numerator and denominator spectra are taken at the same site. It is thus at least possible that influences of local noise sources are eliminated when forming the spectral ratio. Figure 10 indicates that there is no significant effect of the noise amplitudes on the reliability of cover thickness values calculated from H/V main frequencies. This observation strongly suggests the H/V ratio actually is not affected by the presence of local noise sources.

Application

Relationship (11) found for the soft rocks of the western Lower Rhine Embayment enables direct calculations of estimates of sediment thicknesses from the main peak in the microtremor H/V spectral ratios. We demonstrate that this method can be used to obtain information about subsoil geological structure. The cross sections (Fig. 11) show the subsurface structures of the areas investigated. The morphologies of the hard-rock basement shown in the figures were constructed using the data of the microtremor measurements only. The positions of the two profiles are indicated in Figure 5. Profile 1 is situated in the southern area of investigation and extends across the Stolberg Graben. Profile 2 is situated in the northern area of investigation and crosses the Roer Boundary Fault and the Kleingladbach Fault. Cover thicknesses were calculated according to equation (11) for the stations involved. Thicknesses known from drilling are drawn as vertical bars in the profiles. Additionally, the figures contain an interpretation of the geological and tectonic situation.

While in the southeastern part of profile 1, cover thicknesses around 50 m were calculated; thicknesses of up to 200 m can be observed for its northwestern part. This increase of thickness is confirmed by numerous drillings and is due to a northwestern tilt of the Paleozoic basement, as is typical for the blocks of the Lower Rhine Embayment. Additionally, the results of the noise investigations include a strong relief of the basement for the center part of the profile. In this part, not supported by information from drillings, the cover thickness decreases to less than 25 m. This ridge-type high of the basement corresponds well to the assumed position of the Aachen Thrust Fault, a prominent Paleozoic lineament at the base of the Tertiary. The strong relief accompanying the fault results from the different resistance to weathering of the rock types on both sides of the fault. The upper Devonian shale and limestone in the south are less subject to weathering than the upper Carboniferous mudstones and siltstones to the north of the fault. Therefore, the observed structure at the base of the Tertiary can be interpreted as a paleo relief of the postcarboniferous landscape.

Profile 2 is situated in a region of much thicker covers. The results of the noise investigations prove a tilt of the Roer Block in the direction of the Roer Boundary Fault. The thickness calculated for site E6 is 1500 m. Site E7, which is situated only approx. 1 km northeasterly, but beyond the Roer Boundary Fault, proves to have less cover thickness for the Wassenberg Block. Increasing thicknesses beyond the Kleingladbach Fault could also be detected by the measurements. Information from drillings supports the observations. The results of the noise investigations on profile 2 show that also in regions of thick sedimentary covers, the method provides reliable information on thicknesses. Vertical shifts in the basement of more than 1000 m can be detected.

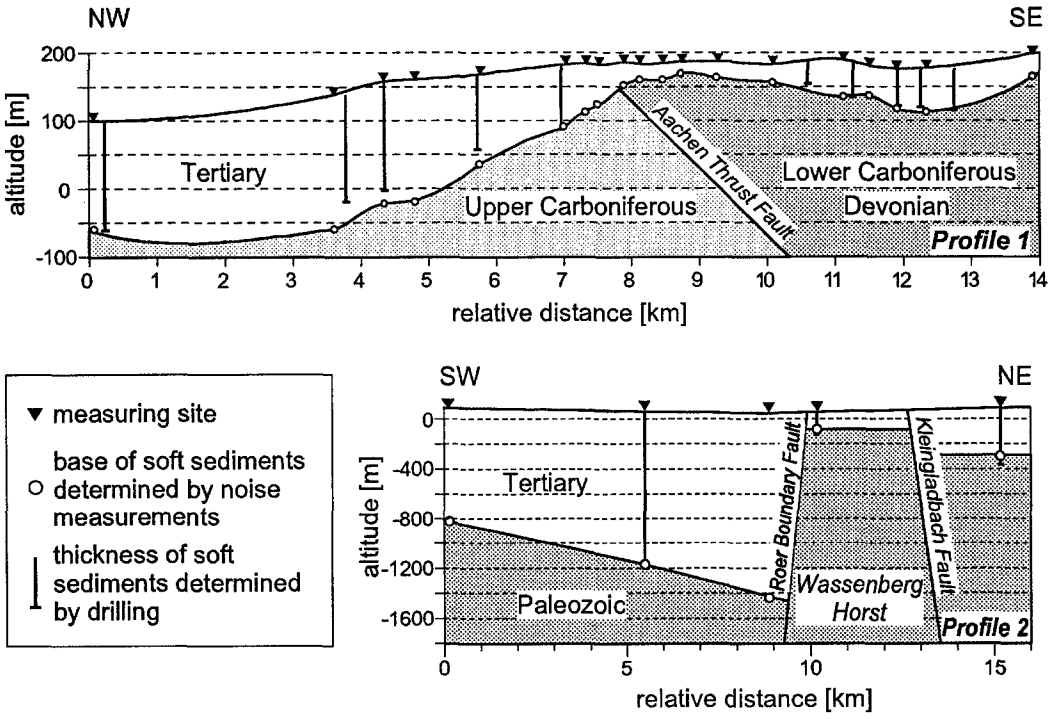

Figure 11. Cross sections showing the subsurface structure of the areas investigated constructed using results of microtremor analysis. For location of profile 1 and profile 2, see Figure 5.

Summary and Conclusions

We have investigated two different spectral ratio techniques that use microtremor recordings for the determination of the fundamental resonant frequency of the subsoil. Our aim was to derive a practical method for mapping the thickness of soft cover layers.

Microtremor measurements taken at 102 sites in the western Lower Rhine Embayment were analyzed using the classical spectral ratio technique and Nakamura's technique. Both approaches reveal spectral ratios that are closely connected to calculated transfer functions of the subsoil. The extensive database of microtremor recordings and the availability of data concerning cover thicknesses derived from drillings allow comparison of the frequency of the main peak in the spectral ratios and the sediment thickness at the measuring sites. Thus, a significant correlation is found to exist between these parameters and a simple formula could be drawn up that calculates estimates of the cover thickness from the spectral ratio main peak. The dependence is clearly controlled by the velocity-depth function of the shear wave, an observation that agrees with the model of resonance in a two-layer case.

The presence of high-amplitude local noise sources strongly influences the shape of the noise spectra and may also spoil the information content of the spectral ratios. Therefore, the two spectral ratio techniques were tested for their sensitivity to noise amplitudes. By comparing cover thicknesses known from drillings and those calculated from the main frequencies in the spectral ratios with respect to the noise level, such a sensitivity becomes evident for the classical spectral ratio technique, whereas Nakamura's technique remains stable.

We conclude that microtremor measurements in combination with Nakamura's technique can be a powerful tool to map sedimentary cover layers. Particularly in regions of unknown basement morphology, such a procedure may be a way to quickly obtain a general idea of the subsurface structure. The requirement for obtaining quantitative thickness values is either knowledge of the velocity-depth function of the shear wave to be assumed for the soft rocks to be measured or an appropriate number of sites with known thicknesses. In the first case, a kind of calibrating function equivalent to equation (11) is to be established using equation (5). In the second case, the function is delivered directly by the measurements at the reference sites. The reliability of the thickness estimates obtained using the calibrating function in the first place is determined by the uniformity of the depth dependence of the shear-wave velocity. The microtremor survey expense is relatively small because only one seismic recorder is required and data processing routines are standard.

Acknowledgments

This study is part of a Ph.D. dissertation at the Institute of Applied Geophysics, Technical University of Aachen. The Deutsche Forschungsgemeinschaft (DFG) supported the research. We thank the reviewers of this article for the constructive comments.

References

Aki, K. and P. G. Richards (1980). *Quantitative Seismology,* vol. I, W. H. Freeman and Company, New York.

Budny, M. (1984). Seismische Bestimmung der bodendynamischen Kennwerte von oberflächennahen Schichten in Erdbebengebieten der Niederrheinischen Bucht und ihre ingenieurseismologische Anwendung, Geological Institute University Cologne, special issue 57.

Field, E. H. and K. H. Jacob. (1990). Using microtremors to assess potential earthquake site response: a case study in Flushing Meadows, New York City, *Bull. Seism. Soc. Am.* **80,** 1456–1480.

Field, E. H. and K. H. Jacob. (1993). The theoretical response of sedimentary layers to ambient seismic noise, *Geophys. Res. Lett.* **20,** 2925–2928.

Field, E. H. and K. H. Jacob. (1995). A comparison and test of various site-response estimation techniques including three that are not reference-site dependent, *Bull. Seism. Soc. Am.* **85,** 1127–1143.

Field, E. H., A. C. Clement, K. H. Jacob, V. Aharonian, S. E. Hough, P. A. Friberg, T. O. Babaian, S. S. Karapetian, S. M. Hovanessian, and H. A. Abramian. (1995). Earthquake site-response study in Giumri (formerly Leninakan), Armenia, using ambient noise observations, *Bull. Seism. Soc. Am.* **85,** 349–353.

Haskell, N. A. (1960). Crustal reflection of plane SH-waves, *J. Geophys. Res.* **65,** 4147–4150.

Lachet, C. and P.-Y. Bard. (1994). Numerical and theoretical investigations on the possibilities and limitations of the "Nakamura's Technique," *J. Phys. Earth* **42,** 377–397.

Lachet, C., D. Hatzfeld, P.-Y. Bard, N. Theodulidis, C. Papaioannou, and A. Savvaidis. (1996). Site effects and microzonation in the city of Thessaloniki (Greece). Comparison of different approaches, *Bull. Seism. Soc. Am.* **86,** 1692–1703.

Lermo, J. and J. Chávez-García. (1993). Site effect evaluation using spectral ratios with only one station, *Bull. Seism. Soc. Am.* **83,** 1574–1594.

Lermo, J. and J. Chávez-García. (1994). Are microtremors useful in site response Evaluation?, *Bull. Seism. Soc. Am.* **84,** 1350–1364.

Lermo, J., M. Rodríguez, and S. K. Singh. (1988). The Mexico earthquake of September 19, 1985—Natural period of sites in the valley of Mexico from microtremor measurements and strong motion data, *Earthquake Spectra* **4,** 805–814.

Nakamura, Y. (1989). A method for dynamic characteristics estimation of subsurface using microtremors on the ground surface, Quarterly Reports of the Railway Technical Research Institute Tokyo, **30,** 25–33.

Steinwachs, M. (1974). Systematische Untersuchungen der kurzperiodischen seismischen Bodenunruhe in der Bundesrepublik Deutschland, *Geologisches Jahrbuch* **E3.**

Technical University of Aachen
Applied Geophysics
Lochnerstrasse 4-20
D-52056 Aachen, Germany

Manuscript received 6 October 1997.